minerals

MDPI

Article

Research on the Adsorption Behavior of Heavy Metal Ions by Porous Material Prepared with Silicate Tailings

Dongxiao Ouyang [1,†], Yuting Zhuo [2,†], Liang Hu [1], Qiang Zeng [1], Yuehua Hu [1] and Zhiguo He [1,*]

[1] School of Minerals Processing and Bioengineering, Central South University, Changsha 410083, China; Ouyangdongxiao@csu.edu.cn (D.O.); huliang2018@csu.edu.cn (L.H.); 165601027@csu.edu.cn (Q.Z.); hyh@csu.edu.cn (Y.H.)

[2] School of Life Science, Central South University, Changsha 410012, China; znyutingzhuo@csu.edu.cn

* Correspondence: zghe@csu.edu.cn

† The first two authors contributed equally to this paper.

Received: 14 March 2019; Accepted: 8 May 2019; Published: 11 May 2019

Abstract: Tailings generated from mineral processing have attracted worldwide concerns due to creating serious environmental pollution. In this work, porous adsorbents were prepared as a porous block by using silicate tailings, which can adsorb heavy metal ions from the solution and are easy to separate. The synthesized silicate porous material (SPM) was characterized by X-ray diffraction (XRD), Brunner–Emmet–Teller (BET), and scanning electron microscope (SEM). The material presented a surface area of 3.40 $m^2 \cdot g^{-1}$, a porosity of 54%, and the compressive strength of 0.6 MPa. The maximum adsorption capacities of Pb^{2+}, Cd^{2+}, and Cu^{2+} by SPM were 44.83 $mg \cdot g^{-1}$, 35.36 $mg \cdot g^{-1}$, and 32.26 $mg \cdot g^{-1}$, respectively. The experimental data were fitted well by the Freundlich and Langmuir adsorption models. The kinetics of the adsorption process were fitted well by the pseudo-first order kinetic equation. These results show that the porous materials prepared with silicate tailings could act as an effective and low-cost adsorbent for the removal of heavy metal ions from wastewater. This study may provide a new thought on the high-value utilization of tailing for alleviating environmental pressure.

Keywords: heavy metals removal; solid waste; silicate porous material; water dispose; recycling

1. Introduction

According to the report of the United Nations Development Program, only one-third of the world's population can get clean water [1], and heavy metal ions are one of the main pollutants that pollute water. Sources of heavy metal pollution are extensive, including paint, electroplating, metal finishing, fertilizer, electrical, pigment industries, and wood manufacturing, etc., which impact on the environment and human health [2]. Various wastewater treatment techniques have been used for the removal of heavy metal ions [3], such as chemical precipitation [4,5], ion exchange [6], adsorption [2,7], membrane filtration [8], and electrochemical treatment [9]. Among these methods, adsorption treatment is considered as a low-cost, high-efficient, eco-friendly, and easily operated method [10,11]. It is of great significance for exploring the proper adsorbents, since the severity of heavy metal pollution and high processing costs are increasing.

Solid waste is another serious environmental issue. Global solid waste production was about 11 billion tons in 2011, and about 1.74 tons solid wastes for per capita were generated in one year [12]. Since rapid urbanization and industrialization need a lot of mineral resources, and these processes will produce vast solid wastes (e.g., tailings), serious environmental problems are then raised. The untreated solid wastes have not only occupied a large area of land resource, but also pollute water and

air if not disposed properly. Landfill was the common method used for disposing waste solid in the past, but this method was inefficient and easily caused secondary pollution [13]. Thus, the secondary utilization of solid waste is a means of effectively relieving environmental pressure and realizing recycling. The use of silicate tailings as an adsorbent is a desired secondary utilization method for solid waste.

There are many studies that investigated the possibility of solid waste for heavy metal adsorption, such as black liquor lignin, slag, flue dust, fly ash, blast furnace sludge, and red mud [14–16]. Similarly, silicate tailings, as an eco-friendly material, were feasible for the removal of various harmful cations due to their wide specific surface area and high adsorption capacity. In recent years, it has been widely studied that natural silicates and modified silicates could be used as potential adsorbents to remove various heavy metal ions from aqueous solvents [17–22]. However, the silicate adsorbents that have been reported were powdered and granulated; these forms of adsorbents were difficult to separate from the solution, and secondary pollution arose easily [23–25]. To find a simple and inexpensive method for separating adsorbents from solution, preparing the adsorbent into a stable structure such as a block with pores is a convenient way to realize this goal [26–28].

Sintering is a simple processing method that has been extensively applied and can observably improve the adsorption capacity of silicate minerals [28]. Sintering minerals at high temperatures can remove the combined water, hydration water, and the water participated in skeleton construction, thus reducing the adsorption resistance of water film to pollutants and increasing its adsorption performance [29]. At the same time, most of the silicate minerals have large specific surface areas, and the surfaces are covered with Al–O– and Si–O–, which could be easily charged and combined with heavy metal ions; these characteristics can also be kept after sintering. Therefore, it is a feasible and beneficial method to sinter silicate tailings into block porous materials to remove heavy metal ions from wastewater.

This work aimed to sinter a bulk porous adsorbent with silicate tailings, which have favorable adsorption capacity and can be easily separated. Meanwhile, the adsorptive behaviors of heavy metals by the synthesized silicate porous material (SPM) were further investigated to evaluate their possible application in the heavy metals containing wastewater.

2. Materials and Methods

2.1. Reagents

The reagents used in this work were all analytical grade. The raw materials for the preparation of SPM were silicate tailings, bauxite, bentonite, $Fe_2(SO_4)_3$, $MgSO_4$, and $NaHCO_3$. The silicate tailing samples of flotation were obtained from Guangdong, China, and the bauxite was obtained from Jiangxi, China. Chemical analysis of the raw materials mentioned above is summarized in Tables 1 and 2. Bentonite with more than 85 wt % of montmorillonite content was obtained from Henan, China. The nitrate solution was dissolved in deionized water to a desired concentration in a stoichiometric amount to prepare a heavy metal ions solution. The pH values of the solution were adjusted by using 0.1 mol·L^{-1} of NaOH or 0.1 mol·L^{-1} of HNO_3 solution, and solution ionic strength was adjusted by using $NaNO_3$ solution.

Table 1. Chemical elemental contents in silicate tailing.

Element Oxide	SiO_2	Al_2O_3	Fe_2O_3	CaO	TiO_2	K_2O	MgO
Chemical composition (%)	73.123	14.095	2.273	1.728	0.229	5.042	0.317

Table 2. Chemical elemental contents in bauxite.

Element Oxide	SiO_2	Al_2O_3	Fe_2O_3	CaO	TiO_2	K_2O	MgO
Chemical composition (%)	28.609	53.231	3.255	2.883	3.734	3.715	1.338

2.2. SPMs Preparation

The SPM was prepared by a sintering method. Silicate tailings and bauxite were milled and sieved through a 200-mesh screen. The raw materials of 64.35 wt % silicate tailings, 27.15 wt % bauxite, 1.35 wt % $Fe_2(SO_4)_3$, 0.92 wt % $MgSO_4$, 1.7 wt % $NaHCO_3$, and 4.53 wt % bentonite were finely mixed, and water (w:v = 10:3.5) was added after mixing the raw materials. A certain amount of the mixture was uniaxially pressed into the mold (length 70 mm, width 50 mm, and height 30 mm) to obtain the green body, which was then placed into the drying oven for 4 h at 80 °C. In the drying process, the green body was expanded with the releasing gas, and the interconnected pores were then formed. Subsequently, the desiccated green body was placed into a muffle furnace with a ramp rate of 10 °C·min^{-1} from the room temperature to 1140 °C and kept for 20 min. After the sintering period, the enamel on the material surface was removed by polishing (Figure S1). All the heat treatments of the green body were conducted with normal pressure and temperature.

2.3. Characterization

Mineralogical analyses of the raw materials and SPM were performed by X-ray diffraction (XRD, SeimensO8DISCOVER, Seimens, Berlin, Germany); the prepared samples were exposed to an X-ray with the 2θ angle varying between 10–80° with Cu Kα radiation. The applied voltage and current were 40 kV and 30 mA, respectively. The major chemical compositions of SPM were analyzed by an X-ray fluorescence (XRF) spectrometer (AxiosmAX Panalytical. B.V, Milford, CT, USA). The microstructure, textural, and morphological characteristics of the SPM sample were observed by the JSM-6460LV scanning electron microscope (Japan electronics corporation, Tokyo, Japan). The specific surface area of the SPM was determined by an automatic specific surface analyzer (Quantachrome Instruments Monosorb, Quantachrome, Düsseldorf, Germany). Fourier transform infrared (FTIR) spectra were recorded on a Nicolet 6700 spectrometer (Nicolet, Waltham, MA, USA). The compressive strengths of the samples, which were cut from the cubes with a normal size of about 20 mm × 20 mm × 20 mm, were measured using an Inst LTD Hydraulic servo dynamic test system 8802 (Instron, London, UK). The porosity of the SPM was measured by a pycnometer and calculated by the formula (Equation (1)):

$$n = \left(1 - \frac{\rho_g}{\rho}\right) \times 100\% \quad (1)$$

where ρ_g is the bulk density, ρ is the true density, and n is the porosity.

2.4. Determination Point of Zero Charge

To determine the point of zero charge [30], a series of 50-mL centrifugal tubes loaded 45 mL of 0.1 mol·L^{-1} of $NaNO_3$ solution were transferred. The solution pH values were adjusted from 2.0 to 10.0 by adding either 0.1 mol·L^{-1} of HNO_3 or 0.1 mol·L^{-1} of NaOH solution. The solution total volume in each flask was adjusted to 50 mL exactly by adding the $NaNO_3$ solution. Then, the pH_0 of the solutions were subsequently recorded. SPM (1 g) was immediately added to each centrifugal tube and securely capped. Then, the suspension was manually agitated, and the pH values of the supernatant liquid were recorded. The differences between the initial and final pH values (pH_0−pH_f) were plotted through the pH_0.

2.5. Adsorption Experiments

Batch mode experiments were conducted on the adsorption of heavy metals by SPM from solutions containing single heavy metal ions at an initial concentration of 125 mg·L^{-1} and an ionic strength of 0.01 mol·L^{-1} of $NaNO_3$ at a temperature of 30 °C. SPM adsorbents that were cut into small cubes (0.5 g) were added into 50-mL capped polyethylene bottles that contained 40 mL of single metal ion solutions; the competitive experiment used 40 mL of multiple metal ion solutions. The bottles were sealed and agitated at 150 revolutions per minute (rpm) in an orbital shaker. The energy-dispersive

spectrum (EDS) was used to confirm that heavy metal ions have been adsorbed on the SPM. After the adsorption process, the mixed solution was centrifuged at 5000 rpm for 10 min, and the supernatant was reserved for Pb^{2+}, Cd^{2+}, and Cu^{2+} analyses by inductively coupled plasma mass spectrometry (ICP-MS, PerkinElmer Elan 6000, PerkinElmer, Waltham, MA, USA). The experimental conditions are shown in Table 3.

Table 3. Batch mode experimental conditions.

Experimental Conditions	Experiment Parameter
Contacting time	Contacting time of 0.5, 1.5, 3.5, 7.5, 11.5, 15.5, 19.5, 24, 26 and 28 h; initial concentration of 125 mg·L^{-1}; pH = 4
Initial heavy metal ions concentrations	Initial heavy metal ions concentrations of 20, 40, 60, 80, 100, 150, 200, 400, 600, 800, 1000, 1200 and 1400 mg·L^{-1}; contacting time 24 h; pH = 4
Initial pH values	Initial pH values of 2, 3, 4, 5, 6 and 7; initial concentration of 125 mg·L^{-1}; contacting time 24 h
Competitive adsorption	Contain Pb^{2+}, Cd^{2+} and Cu^{2+} of 20, 40, 60, 80 and 100 mg·L^{-1}, respectively; contacting time 24 h

All the experiments were performed in triplicate, and the procured data were analyzed by Origin 8.0 (OriginLab, Northampton, MA, USA). The adsorption amounts of heavy metal ions at equilibrium state were calculated using Equation (2), and the removal efficiency was calculated using Equation (3).

$$q_e = \frac{(Co - Ce)V}{M}, \tag{2}$$

$$\text{Removal efficiency} = \frac{C_0 - C_e}{C_0} \times 100\%, \tag{3}$$

where q_e is the adsorption capacity (mg·g^{-1}), C_0 is the initial concentration of a heavy metal (mg·L^{-1}); C_e is the equilibrium concentration of a heavy metal (mg·L^{-1}); V is the volume of solution (L), and M is the mass of adsorbent (g). The average value was obtained, and the error ranges were controlled within ±5%. The amount of each ion adsorbed on SPM was calculated and expressed as a percentage by using the difference between the amount of ion in the initial solution and the final solution.

2.6. Desorption Experiments

The desorption experiments were carried out with 0.1 mol·L^{-1} of HNO_3 solution. First, 0.5 g of SPM loaded with single heavy metals after adsorption was dried in the oven. After drying, the SPM was added into 40 mL of HNO_3 solution and shaken in a shaker at 30 °C for 24 h. Next, the mixture was centrifuged at 4000 rpm for 10 min, and the SPM precipitant was collected. The amount of desorbed heavy metal ions was determined by the amount of heavy metal ions in the solution.

2.7. Adsorption Isotherm of SPM

Langmuir and Freundlich adsorption isotherm models were used to depict the equilibrium between adsorbed Pb^{2+}, Cd^{2+}, and Cu^{2+} on SPM (q_e) and ions concentration in solution (C_e) at constant temperature (30 °C). The ratio of adsorbent to solution volume was 12.5 g·L^{-1}, and the adsorption amount kept rising during heavy metal ions concentration ranging from 20 mg·L^{-1} to 1000 mg·L^{-1}.

2.8. Kinetic Study of SPM

The pseudo-first order and pseudo-second order kinetic models were used to describe the adsorption process at a heavy metal ions concentration of 125 mg·L^{-1} and temperature of 30 °C. The ratio of adsorbent to solution volume was 12.5 g·L^{-1}. The removal rate of heavy metals in the solution was increased with time from 0 to 28 h.

2.9. Column Experiments

The columns were constructed from a polymethyl methacrylate cylinder (inner diameter 25 mm, length 100 mm) which were packed with 16 g of SPM to yield a bed height of 90 mm. Single heavy metal ions solution with a concentration of 100 mg·L^{-1} was pumped upward through the column at a filtration velocity of 5 mL·min^{-1} and controlled by a peristaltic pump.

3. Results and Discussion

3.1. Characterization of the SPM

The zero-charge point was determined by the solid addition method, and the zero-charge point (pH_0) of SPM was 6.7 (Figure 1a). The XRD patterns of SPM, bauxite, and tailings are shown in Figure 1b. The crystalline phases of raw materials were mainly composed of quartz, orthoclase, and diaspore. After the sintering process, the main crystalline phases of SPM were quartz, corundum, and hematite, which have been previously shown to be capable of adsorbing heavy metal ions [31–33].

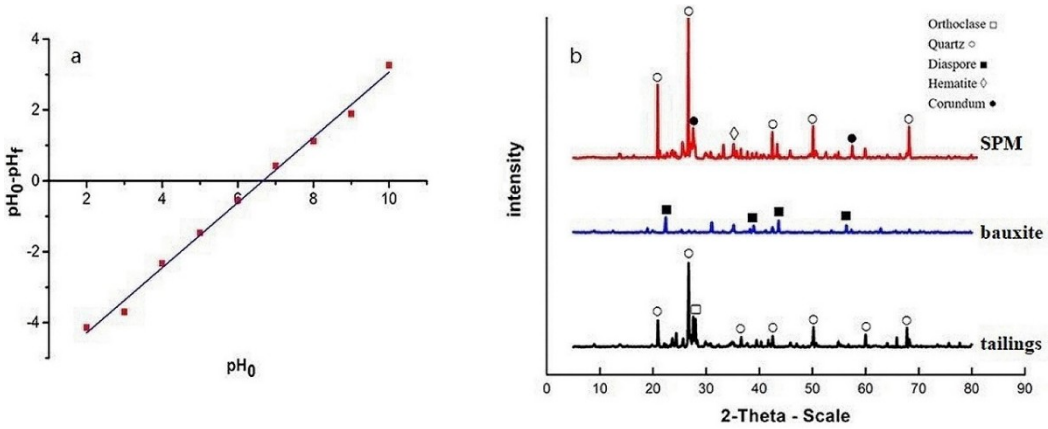

Figure 1. Zero-charge point of the silicate porous material (SPM) (Figure 1**a**) and X-ray diffraction (XRD) patterns of SPM, bauxite, and tailings (Figure 1**b**, red for SPM, blue for bauxite, and black for tailings).

Based on the BET analysis, the SPM has a specific surface area of 3.40 $m^2 \cdot g^{-1}$, and a porosity of 54%. The compressive strength of SPM is 0.6 MPa. The above characteristics of SPM basically accorded with the design requirements. SEM was used to observe the morphology of SPM, which was shown in Figure 2. Some favorable features of SPM were found; the material surface had geometrical properties with irregular shape and large agglomerates and the rugged surface, which would provide more sites for adsorbing heavy metal ions.

The FTIR spectra of SPM, silicate tailings, bauxite, and bentonite were shown in Figure 3. The peaks of these substances were mainly distributed in three regions: 3399–3695 cm^{-1}, 1608–1873 cm^{-1}, and 542–792 cm^{-1}. The characteristic absorption peaks at 3399 cm^{-1} and 3695 cm^{-1} were assigned to the Si–OH stretching vibration [30]. The peaks at 1629 cm^{-1} and 1873 cm^{-1} were attributed to C–O lattice vibrations [34]. The adsorption bond at 542 cm^{-1} represented the Si–O stretching vibration, and the adsorption bonds near 534–542 cm^{-1} were –H deformation vibration [35]. The Si–O symmetric stretching vibration occurred at 792 cm^{-1} [33,36]. The broad bonds near 1034–1047 cm^{-1} were assigned to stretching vibrations of the Si–O tetrahedral [36]. The peaks located at about 3695 cm^{-1} and 1822 cm^{-1} were approximately the Mg_3O–H and Fe–O stretching vibrations in the spectra of SPM. Mg_3O–H and Fe–O are presented in SPM, because $MgSO_4$ and $Fe_2(SO_4)_3$ were added during the preparation [35,37]. In the spectra of raw materials, included silicates, tailings, bentonite, and bauxite, peaks of C–O stretching vibration located at 1608–1629 cm^{-1}, 1871–1873 cm^{-1}, 1989 cm^{-1} and 2123 cm^{-1} were observed [37], which might be due to the existed impurities or a small amount of adsorbing carbon dioxide. The adsorption bonds of C–O at 1989 cm^{-1} and 2128 cm^{-1} disappeared in SPM, which

could be due to the bicarbonate decomposition at high temperatures. Therefore, it could be concluded that the hydroxyl groups on the surface of SPM played an important role in the removal of heavy metals [38].

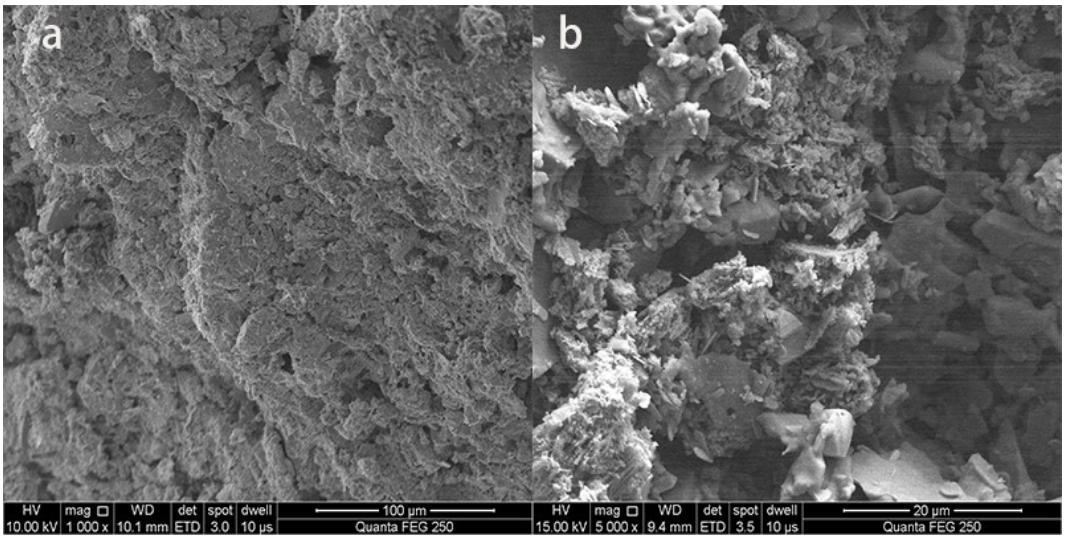

Figure 2. Micromorphology of SPM 1000× (**a**) and 5000× (**b**).

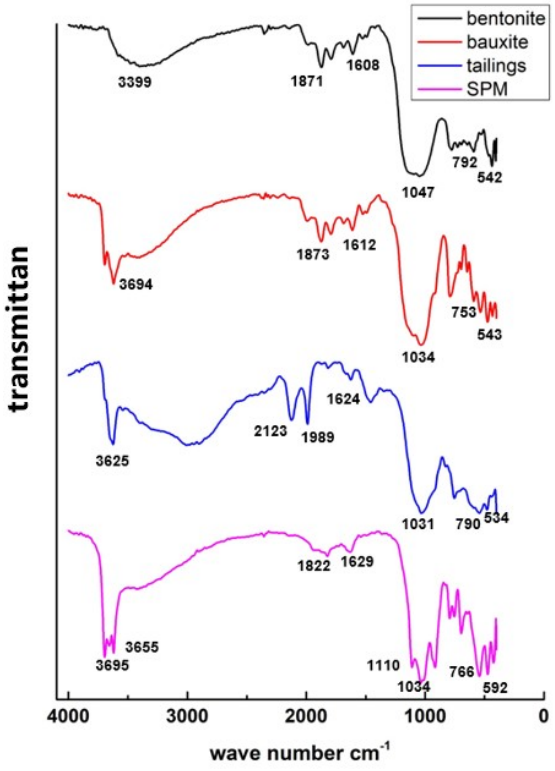

Figure 3. Fourier transform infrared (FTIR) spectra of SPM, silicate tailings, bauxite, and bentonite.

3.2. *Adsorption Properties*

3.2.1. Effect of Contacting Time

The uptake capacities of single heavy metal ions were investigated as a function of time to determine an optimum contact time for the adsorption of heavy metal ions on SPM. The effects

of contact time on adsorption amount of Pb^{2+}, Cd^{2+}, and Cu^{2+} by SPM are shown in Figure 4. The equilibrium time was found to be 20 h. At equilibrium conditions, 88.4% of Pb^{2+}, 51.2% of Cd^{2+}, and 41.3% of Cu^{2+} were removed from the solution. When interacting with heavy metal ions, the adsorption site on SPM gradually decreased, but the percentage of adsorption depended on the amount of heavy metal ions transported from the bulk liquid phase to the actual adsorption site, so the percentage of adsorption increased with time until saturation [39]. SPM could remove these heavy metal ions at different extents, and the removal abilities of different metal ions were in the order of Pb^{2+} > Cd^{2+} > Cu^{2+}, which could be due to the difference in the ion-exchange capacity of the heavy metal ions adsorbed on SPM [40]. EDS results confirmed that Pb^{2+}, Cd^{2+}, and Cu^{2+} were adsorbed on the SPM surface. As shown in Figure S2, the characteristic peaks of Pb, Cd, and Cu were observed in the EDS spectra, and the corresponding peak intensities on the energy spectra were increased compared to blanks. The removal percentage remains stagnant at 0.5 to 4 h, which might be contributed by the tiny and rich micropores filled in SPM. After the addition of SPM, the heavy metal ions were rapidly adsorbed onto the external surface of the SPM, since the external surface was in direct contact with the solution. Owing to the narrow diameter of micropores, the heavy metal ions needed more time to permeate into the pores, so it took a long time for SPM to get the adsorption saturation. Therefore, the first time to reach equilibrium could indicate the adsorption saturation of the outer surface, and the second equilibrium was probably the adsorption saturation of the inner surface of the pores. The amount of adsorption when reaching the second equilibrium is significantly higher than that of the first time. It could be inferred that the amount of heavy metal ions adsorbed on the internal surface of SPM was more than that adsorbed on the external surface.

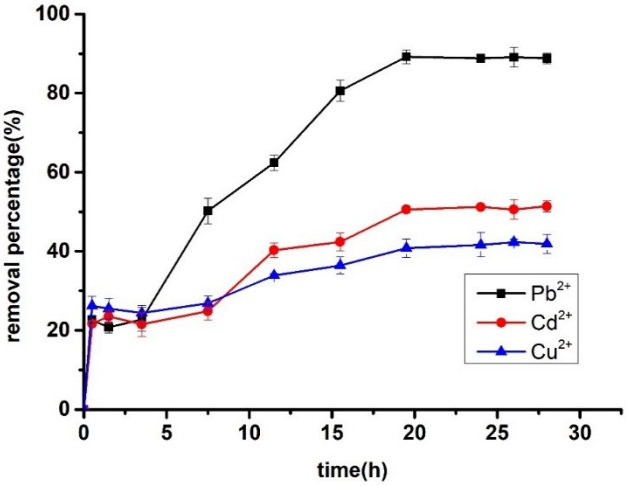

Figure 4. Effect of contact time on the adsorbed amount of Pb^{2+}, Cd^{2+}, and Cu^{2+} at an initial concentration of 125 mg·L^{-1}, agitation speed of 150 rpm, each adsorbent dose of 12.5 g·L^{-1}, and temperature of 30 °C.

3.2.2. Effect of Initial Concentration of Heavy Metal Ions

The influence of initial concentrations of heavy metal ions on the adsorption of Pb^{2+}, Cd^{2+}, and Cu^{2+} by SPM was investigated, and the results are shown in Figure 5. The adsorption capacity sharply increased with the increase of the initial concentration of heavy metals ions ranging from 20 mg·L^{-1} to 1000 mg·L^{-1}. The maximum adsorption capacities of Pb^{2+}, Cd^{2+}, and Cu^{2+} by SPM were 44.83 mg·g^{-1}, 35.36 mg·g^{-1}, and 32.26 mg·g^{-1}, respectively. The adsorption capacity of heavy metal ions increased, and the removal efficiency decreased with the increasing initial concentrations of heavy metal ions [39]. This indicated that the increase of initial concentrations of heavy metal ions contributed to enhance the driving force at the solid–liquid interface to increase the adsorption capacity until the adsorption sites were saturated [41,42]. In order to describe the adsorption behaviors well (i.e., the extent of adsorption

and relevant mechanism), the experimental data were then fitted with the Freundlich and Langmuir isotherm models in Section 3.5.

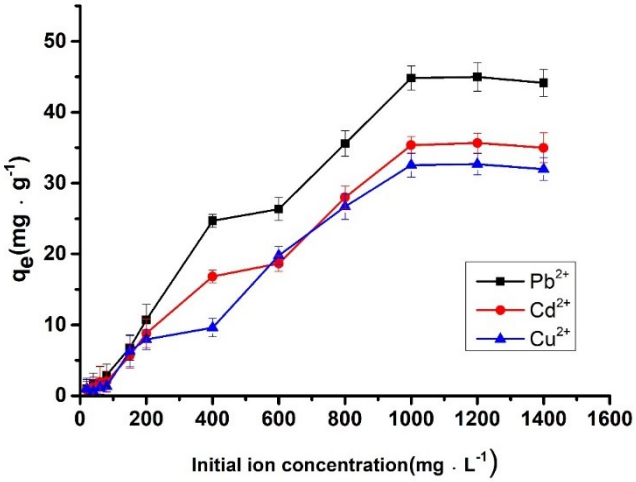

Figure 5. Adsorption isotherms for Pb^{2+}, Cd^{2+}, and Cu^{2+} on the adsorbents at heavy metal ions concentrations from 20 to 1400 mg·L^{-1}, an adsorbent dose of 12.5 g·L^{-1}, an agitation speed of 150 rpm, a temperature of 30 °C, and a contact time of 24 h.

3.2.3. Effect of pH Value on the Adsorption of Heavy Metal Ions

During the adsorption process, the pH value is one of the important impact factors that can influence the heavy metal ions binding to the surface of the adsorbent, since the pH value of the solution would affect the binding sites on the surface of the adsorbent and the chemical nature of the adsorbent, and the hydrogen ions could strongly compete with heavy metal ions at low pH values [43,44]. In this work, the effect of pH value on the adsorption of heavy metal ions was investigated, and the results are shown in Figure 6. The adsorption curve results indicated that the effect of pH value on Cd^{2+} adsorption was not distinct, but the effect was obvious for Pb^{2+} and Cu^{2+}, and the removal efficiency increased as the pH value increased from 2 to 6. The removal efficiencies of Pb^{2+} and Cd^{2+} reached their maximum of 82% and 71% at pH 6, respectively, while the removal efficiencies dropped down to 57% and 63% when the pH value was higher than 6. The removal efficiency of Cu^{2+} reached a maximum of 98% at pH 7. The surface of SPM contained many active sites, and might become positively charged at a low pH value, thus increasing the competition between the heavy metal ions and H^+ for available adsorption sites. However, this competition decreased while these surface active sites became more negatively charged with the increasing pH value, which enhanced the adsorption of the positively charged metal ions through electrostatic force [45,46]. To rule out the effect of SPM on the pH of the solution, the results are shown in Table S1 and Figure S3. The adsorption results of SPM in this study are consistent with most of the previously reported silicate minerals. The Cu^{2+} removal efficiency of 98% from the solution at pH 7 was attributed to Cu^{2+} being favored to precipitate as $Cu(OH)_2$ when the pH value was above 6 [39]. This phenomenon further proved that electrostatic interaction played an important role in the adsorption of Pb^{2+}, Cd^{2+}, and Cu^{2+}. Thus, the optimal pH value for the removal of Pb^{2+}, Cd^{2+}, and Cu^{2+} was determined to be 6 in this study.

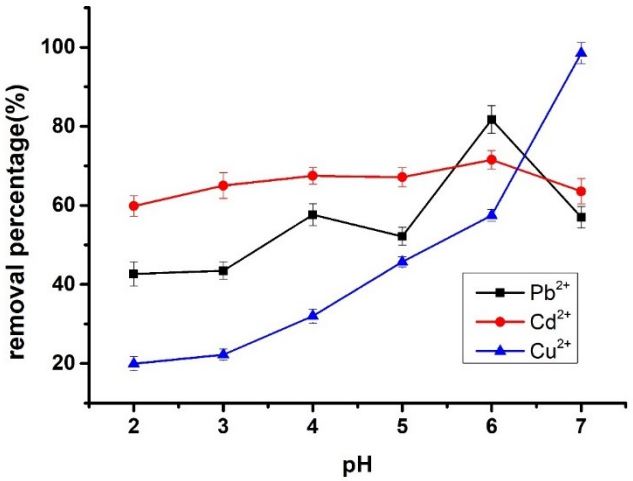

Figure 6. Effect of pH value on the adsorption of Pb^{2+}, Cd^{2+}, and Cu^{2+} onto the adsorbents at an ion concentration of 125 mg·L^{-1}, an adsorbent dose of 12.5 g·L^{-1}, an agitation speed of 150 rpm, a solution temperature of 30 °C, and a contact time of 24 h.

3.2.4. Competitive Adsorption among Three Heavy Metal Ions

It is of great significance to investigate the interaction between heavy metal ions and SPM, since various heavy metal ions usually coexist in the wastewater. The effects of interaction among heavy metal ions on the adsorption of Pb^{2+}, Cd^{2+}, and Cu^{2+} were tested, and the results are shown in Figure 7. When the initial concentration of metal ions increased from 20 mg·L^{-1} to 100 mg·L^{-1}, the removal efficiency of heavy metal ions decreased significantly. The result indicated that the adsorption amount presented a significant difference between single metal and multi-metal ions adsorbed on the SPM. The adsorption capacity of Pb^{2+} was larger than those of Cd^{2+} and Cu^{2+}. For example, the 42.8% of Pb^{2+} was adsorbed on the SPM when the multi-metal ions concentration was 100 mg·L^{-1}, but the removal efficiencies of Cd^{2+} and Cu^{2+} were just 13.8% and 4.9% at the same concentration, respectively. In single metal experiments, the removal efficiencies of Pb^{2+}, Cd^{2+}, and Cu^{2+} were higher than those of multi-heavy metal ions experiments at the same concentration. Since different heavy metal ions competed for adsorption sites, the removal efficiency in a single-metal system was higher than that of a multi-metal ions system. The higher concentration of mixed heavy metal ions resulted in the stronger competition among heavy metal ions. Pb^{2+} could replace Cd^{2+} and Cu^{2+} to be adsorbed on the surface of the SPM; therefore, Pb^{2+} was more competitive than Cd^{2+} and Cu^{2+} [47]. These different properties of heavy metal ions, such as ionic potential, electronegativity, softness capacity for hydroxylation, and position in the Irving–Williams series [48] also made the difference in removal efficiency among heavy metal ions adsorption. The preference of the sorbent for the Pb^{2+} may be because the metal ions have the largest atomic weight and paramagnetic, and the most electronegative ion has the highest standard reduction potential as compared to Cu^{2+} and Cd^{2+} [49]. Another reason may be related to the hydration energy and hydrated ionic radius of heavy metals, and the lower hydration energy was easier for the adsorption. The hydration energy ranked as follows: $Pb^{2+} < Cd^{2+} < Cu^{2+}$ [36].

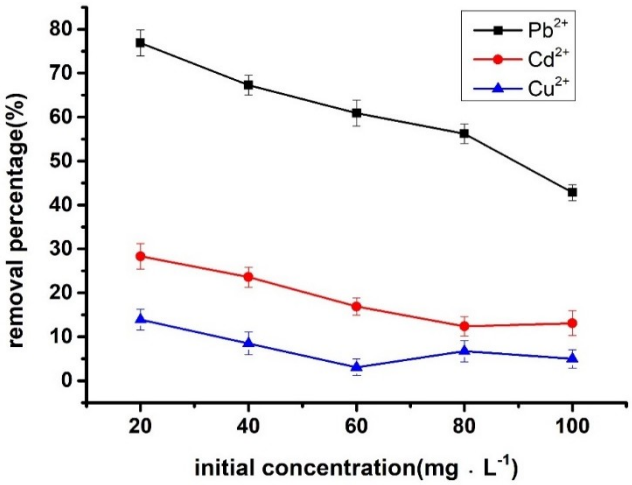

Figure 7. Competitive adsorption of Pb^{2+}, Cd^{2+}, and Cu^{2+} on the adsorbents at a heavy metal ions concentration of 100 mg·L^{-1}, each adsorbent dose of 12.5 g·L^{-1}, agitation speed of 150 rpm, temperature of 30 °C, and contact time of 24 h.

3.3. Desorption of Heavy Metal Ions

The result of single heavy metal ions desorption from SPM is shown in Figure 8. During the desorption process, Cd^{2+} and Cu^{2+} presented greater desorption efficiency than Pb^{2+}. Heavy metal ions were released from the surfaces of SPM over the first nine hours of the desorption process, and 15.8% of Cd^{2+}, 16.7% of Cu^{2+}, and 35.8% of Pb^{2+} were desorbed from SPM, respectively. The loosely bound metal from the surface of the adsorbent could not be washed away before the desorption experiment, so a very strong desorption occurred at the beginning of the desorption experiment. The desorption isotherm indicated that Cd^{2+} and Cu^{2+} could be strongly bonded on the surface of the SPM, which should be due to the existence of sites for specifically adsorbing Cd^{2+} and Cu^{2+} on the SPM surface. This result indicated that more Cd^{2+} and Cu^{2+} could be adsorbed on specific sites than nonspecific sites, while a higher proportion of Pb^{2+} was adsorbed on a non-specific site [40]. This also indicated that more non-specific sites were on the SPM surface, leading to the better adsorption capacity for Pb^{2+} by SPM, but the binding stability for Pb^{2+} was lower as compared with those of Cd^{2+} and Cu^{2+} [48].

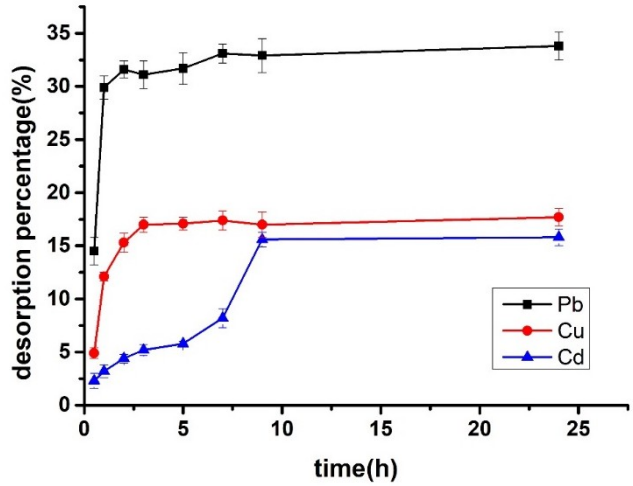

Figure 8. The desorption behaviors of Pb^{2+}, Cu^{2+}, and Cu^{2+} from SPM after successive desorption.

The raw material for the preparation of SPM was silicate tailings, and the main components were the silicate with great adsorption capacity to heavy metals ions. Table 4 shows the adsorption results

of reports on various silicate solid wastes. Compared with silicate solid wastes, SPM was sintered into block, which retained the excellent adsorption capacity of silicate solid wastes and was easy to separate from solution, avoiding secondary pollution. Thus, the preparation of SPM provides a way for reusing solid waste such as silicate tailings.

Table 4. Adsorption of metals on other silicate solid wastes.

Adsorbent	Ions	Adsorption Capacity	References
Natural clay	Cu^{2+}	10.8 mg·g^{-1}	[49]
Smectite-rich clay	Pb^{2+}	25.44 mg·g^{-1}	[31]
Bentonite	Cu^{2+}	42.41 mg·g^{-1}	[36]
Coal fly ash	Cd^{2+}	18.98 mg·g^{-1}	[50]
Fly ash	Pb^{2+}	18.8 mg·g^{-1}	[51]
Fly ash zeolite	Pb^{2+}	70.6 mg·g^{-1}	[52]
Blast furnace slag	Pb^{2+}	40.0 mg·g^{-1}	[53]
Blast-furnace sludge	Cd^{2+}	16.07 mg·g^{-1}	[54]
Coal fly ash	Cu^{2+}	20.92 mg·g^{-1}	[55]
Treated sewage sludge	Cd^{2+}	16.7 mg·g^{-1}	[56]
SPM	Pb^{2+}	44.83 mg·g^{-1}	The study
	Cd^{2+}	35.36 mg·g^{-1}	
	Cu^{2+}	32.26 mg·g^{-1}	

3.4. Adsorption Isotherm of SPM

The adsorption equilibriums are usually described by isotherm equations whose parameters represent the surface properties and affinity of the adsorbent. The adsorption isotherms can be generated on the basis of theoretical models, the most common of which are the Langmuir model and the Freundlich model [45]. The Langmuir (Equation (4)) and Freundlich (Equation (5)) adsorption isotherm models can be written as follows:

$$\frac{C_e}{q_e} = \frac{1}{q_m k_l} + \frac{C_e}{q_m} \tag{4}$$

$$\ln q_e = lnk_f + \frac{1}{n} lnC_e \tag{5}$$

The Langmuir and Freundlich models can describe the adsorption mechanism on the surface well, and they can account for these experimental results in a wider range concentration [57,58]. According to the Langmuir adsorption model and Freundlich adsorption model, the values of q_e followed the sequence: $Pb^{2+} > Cd^{2+} > Cu^{2+}$, which matched to the batch experiment. In fact, the data obtained from the experiment of adsorption fitted the two models well (Table 5), indicating that the adsorption sites were uneven and non-specific. The adsorption coefficient is greatly consistent with the conditions that support favorable adsorption. This result suggested that more than one type of active site took part in the heavy metal ions adsorption, such as some specific adsorption sites that were consistent with the speculation of Section 3.3 [42].

Table 5. Langmuir model and Freundlich model parameters.

Ions	Langmuir Model				Freundlich Model		
	q_{max}	k_L	b *	R^2	k_F	n	R^2
Pb^{2+}	44.832	0.068	17.732	0.982	2.473	0.992	0.984
Cd^{2+}	35.368	0.071	15.453	0.984	3.229	0.946	0.983
Cu^{2+}	32.561	0.038	13.367	0.981	4.183	0.853	0.981

* b is equilibrium constant for Langmuir model.

3.5. Kinetic Study of SPM

The pseudo-first order kinetic model and pseudo-second order kinetic model have been diffusely used to describe the removal of pollutants from solution in different fields [28]. Here, the tested pseudo-first order (Equation (6)) and pseudo-second order (Equation (7)) kinetics models can be written as follows:

$$ln(q_e - q_t) = lnq_e - k_1 t \quad (6)$$

$$\frac{t}{q_t} = \frac{1}{k_2 {q_e}^2} + \frac{t}{q_e} \quad (7)$$

where q_e is the mass of heavy metal ions adsorbed at equilibrium (mg·g^{-1}), q_t is the mass of metal adsorbed at time t (h), and k_1 and k_2 are the pseudo-first order model and the pseudo-second order model rate constants of adsorption. The kinetic adsorption data were satisfactorily fitted to the pseudo-first order model and pseudo-second order model (Table 6). The R^2 values of the pseudo-first order model and pseudo-second order model for Pb^{2+}, Cd^{2+}, and Cu^{2+} were ~0.915–0.984 and ~0.908–0.982, respectively, and the equilibrium adsorption capacities predicted from the models were approximately equal to the corresponding experimental values. The diffusion process of heavy metal ions will affect the interaction between heavy metal ions and the SPM surface; thus, the adsorption rate will be affected. If the R^2 values were considered, the pseudo-first order model appeared to fit the data better than the pseudo-second order model. The better-fitted results suggested that the diffusion process might be the prior rate-limiting step in the adsorption.

Table 6. Pseudo-first order kinetic model and pseudo-second order kinetic model parameters.

Ions	Pseudo-First Order Kinetic Model			Pseudo-Second Order Kinetic Model		
	q_e	k_1	R^2	q_e	k_2	R^2
Pb^{2+}	44.832	0.068	0.982	4.439	0.051	0.908
Cd^{2+}	35.368	0.071	0.984	2.57	0.128	0.943
Cu^{2+}	32.561	0.038	0.981	2.093	0.278	0.982

3.6. Column Experiments

Column experiments were conducted for determining the single ion adsorption characteristics of Pb^{2+}, Cd^{2+}, and Cu^{2+} in the dynamic adsorption process, respectively (Figure 9), and the adsorption parameters are listed in Table 7. The Thomas model satisfactorily described the adsorption behavior of the different heavy metal ions from SPM (R^2 = 0.913~0.934). SPM had better adsorption ability for Pb^{2+} as compared to Cd^{2+} and Cu^{2+} in the column experiments, and the time to reach the plateau of Ct/C0 value was significantly longer for Pb^{2+} than other metal ions. The results can be obtained from Figure 8 that the breakthrough speed was the slowest and the adsorption curve was the least steep for Pb^{2+}. The breakthrough point of Cu^{2+} appeared at about 30 min, followed by Cd^{2+} at 60 min and Pb^{2+} at 110 min. The adsorption capacity order of the column from the breakthrough curves was $Pb^{2+} > Cd^{2+} > Cu^{2+}$, which suggested that Pb^{2+} was the most easily to bond to the adsorption sites of SPM in the column experiment. This is consistent with the results of the batch experiment, because Pb^{2+} presented stronger adsorption properties due to its greater ion size, while Cu^{2+} and Cd^{2+} were lower affinity to bind to the adsorption groups [59]. The maximal capacity of the column experiment was significantly lower than that of the batch experiment, because the heavy metal ions flowing through the columns probably had less contact time, and the adsorption equilibrium was not reached, unlike in the batch equilibrium experiment [60]. Therefore, SPM is an appropriate adsorbent to adsorb heavy metal ions from the contaminated aqueous media in column adsorption application.

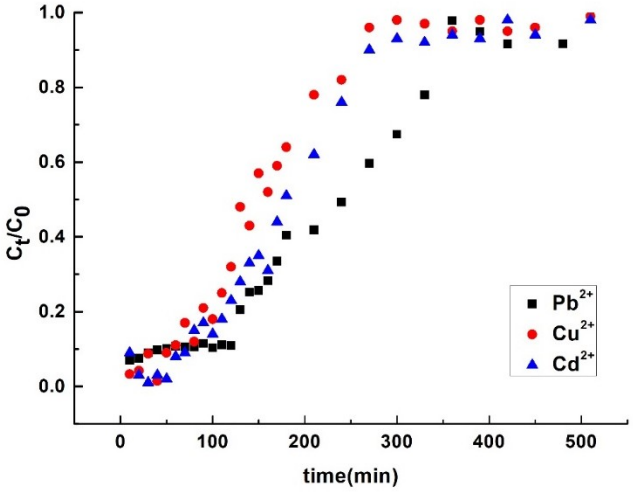

Figure 9. Adsorption curves of column experiments.

Table 7. Thomas model parameters.

Ions	q_e (mg·g^{-1})	k_{th}	R^2
Pb^{2+}	14.421	0.072	0.926
Cd^{2+}	13.025	0.069	0.934
Cu^{2+}	11.653	0.061	0.913

4. Conclusions

Preparing the silicate tailings into foamed silicate porous materials for heavy metal adsorption from solution is an effective way to alleviate environmental pressures from tailings, and can attain sustainability. Porous materials were successfully fabricated by silicate tailings in this work, and it could be used as an adsorbent to remove Pb^{2+}, Cd^{2}, and Cu^{2+} from aqueous solution with high adsorption capacities. The adsorption performance of SPM was greatly affected by the pH value and the other co-existence of heavy metal ions in the solution. Referring to the heavy metal ions on the SPM, the selective adsorption order of these metals was $Pb^{2+} > Cd^{2+} > Cu^{2+}$. In addition, experimental data were suitable for the Langmuir model and the Freundlich model, indicating that the adsorption sites were uneven and less non-specific. The kinetic model fitting results indicated that the adsorption process was limited by heavy metal ions diffusion and chemisorption processes. The experimental results indicate that the SPM prepared in this study is a potential adsorbent for the removal of heavy metal ions from solution.

Supplementary Materials: The following are available online at http://www.mdpi.com/2075-163X/9/5/291/s1, Figure S1: Photographs of SPM, Figure S2: EDS spectra of SPM after adsorb heavy metal ions (a-Pb, b-Cd, c-Cu, d-blank), Figure S3: Effect of pH value on the ion concentration, Table S1: The effect of SPM on the initial concentration of the solution.

Author Contributions: Z.H. and Y.H. received the project; Z.H. designed the experiment; D.O. performed the experiment; D.O., Y.Z. and Q.Z. analyzed the data; D.O., Y.Z. and L.H. wrote and revised the manuscript, respectively.

Funding: This work was supported by the National Natural Science Foundation of China (31500091 and 51774339), Co-Innovation Center for Clean and efficient Utilization of Strategic Metal Mineral Resources.

Conflicts of Interest: The authors declare no conflict of interest.

References

1. Alqadami, A.A.; Naushad, M.; Abdalla, M.A.; Ahamad, T.; Abdullah ALOthman, Z.; Alshehri, S.M.; Ghfar, A.A. Efficient removal of toxic metal ions from wastewater using a recyclable nanocomposite: A study of adsorption parameters and interaction mechanism. *J. Clean. Prod.* **2017**, *156*, 426–436. [CrossRef]
2. Manzoor, Q.; Nadeem, R.; Iqbal, M.; Saeed, R.; Ansari, T.M. Organic acids pretreatment effect on Rosa bourbonia phyto-biomass for removal of Pb(II) and Cu(II) from aqueous media. *Bioresour. Technol.* **2013**, *132*, 446–452. [CrossRef]
3. Fu, F.; Wang, Q. Removal of heavy metal ions from wastewaters: A review. *J. Environ. Manag.* **2011**, *92*, 407–418. [CrossRef] [PubMed]
4. Wang, X.; Jing, S.; Hou, Z.; Liu, Y.; Qiu, X.; Liu, Y.; Tan, Y. Permeable, robust and magnetic hydrogel beads: Water droplet templating synthesis and utilization for heavy metal ions removal. *J. Mater. Sci.* **2018**, *53*, 15009–15024. [CrossRef]
5. Ku, Y.; Jung, I.L. Photocatalytic reduction of Cr(VI) in aqueous solutions by UV irradiation with the presence of titanium dioxide. *Water Res.* **2001**, *35*, 135–142. [CrossRef]
6. Kang, S.-Y.; Lee, J.-U.; Moon, S.-H.; Kim, K.-W. Competitive adsorption characteristics of Co^{2+}, Ni^{2+}, and Cr^{3+} by IRN-77 cation exchange resin in synthesized wastewater. *Chemosphere* **2004**, *56*, 141–147. [CrossRef] [PubMed]
7. Castro, L.; Blázquez, M.L.; González, F.; Muñoz, J.A.; Ballester, A. Hydrometallurgy Heavy metal adsorption using biogenic iron compounds. *Hydrometallurgy* **2018**, *179*, 44–51. [CrossRef]
8. Landaburu-Aguirre, J.; García, V.; Pongrácz, E.; Keiski, R.L. The removal of zinc from synthetic wastewaters by micellar-enhanced ultrafiltration: Statistical design of experiments. *Desalination* **2009**, *240*, 262–269. [CrossRef]
9. Zhou, L.; Xiong, W.; Liu, S. Preparation of a gold electrode modified with Au–TiO_2 nanoparticles as an electrochemical sensor for the detection of mercury(II) ions. *J. Mater. Sci.* **2015**, *50*, 769–776. [CrossRef]
10. Gong, R.; Sun, Y.; Chen, J.; Liu, H.; Yang, C. Effect of chemical modification on dye adsorption capacity of peanut hull. *Dyes Pigment.* **2005**, *67*, 175–181. [CrossRef]
11. Yen, C.H.; Lien, H.L.; Chung, J.S.; Yeh, H. Der Adsorption of precious metals in water by dendrimer modified magnetic nanoparticles. *J. Hazard. Mater.* **2017**, *322*, 215–222. [CrossRef]
12. Song, Q.; Li, J.; Zeng, X. Minimizing the increasing solid waste through zero waste strategy. *J. Clean. Prod.* **2015**, *104*, 199–210. [CrossRef]
13. Petcherdchoo, A. Repairs by fly ash concrete to extend service life of chloride-exposed concrete structures considering environmental impacts. *Constr. Build. Mater.* **2015**, *98*, 799–809. [CrossRef]
14. Zhang, L.; Zeng, Y.; Cheng, Z. Removal of heavy metal ions using chitosan and modified chitosan: A review. *J. Mol. Liq.* **2016**, *214*, 175–191. [CrossRef]
15. Ahmaruzzaman, M. Industrial wastes as low-cost potential adsorbents for the treatment of wastewater laden with heavy metals. *Adv. Colloid Interface Sci.* **2011**, *166*, 36–59. [CrossRef]
16. Lee, B.; Kim, Y.; Lee, H.; Yi, J. Synthesis of functionalized porous silicas via templating method as heavy metal ion adsorbents: The introduction of surface hydrophilicity onto the surface of adsorbents. *Microporous Mesoporous Mater.* **2001**, *50*, 77–90. [CrossRef]
17. You, W.; Hong, M.; Zhang, H.; Wu, Q.; Zhuang, Z.; Yu, Y. Functionalized calcium silicate nanofibers with hierarchical structure derived from oyster shells and its application in heavy metal ions removal. *Phys. Chem. Chem. Phys.* **2016**, *18*, 15564–15573. [CrossRef]
18. Huang, R.; Wu, M.; Zhang, T.; Li, D.; Tang, P.; Feng, Y. Template-free Synthesis of Large-Pore-Size Porous Magnesium Silicate Hierarchical Nanostructures for High-Efficiency Removal of Heavy Metal Ions. *ACS Sustain. Chem. Eng.* **2017**, *5*, 2774–2780. [CrossRef]
19. Huang, R.; He, L.; Zhang, T.; Li, D.; Tang, P.; Feng, Y. Novel Carbon Paper @ Magnesium Silicate Composite Porous Films: Design, Fabrication, and Adsorption Behavior for Heavy Metal Ions in Aqueous Solution. *ACS Appl. Mater. Interfaces* **2018**, *10*, 22776–22785. [CrossRef] [PubMed]
20. Petrella, A. Porous Alumosilicate Aggregate as Lead Ion Sorbent in Wastewater Treatments. *Separations* **2017**, *4*, 25. [CrossRef]
21. Kim, J.; Kwak, S. Efficient and selective removal of heavy metals using microporous layered silicate AMH-3 as sorbent. *Chem. Eng. J.* **2016**, *313*, 975–982. [CrossRef]

22. Chen, J.; He, F.; Zhang, H.; Zhang, X.; Zhang, G.; Yuan, G. Novel core-shell structured Mn-Fe/MnO_2 magnetic nanoparticles for enhanced Pb(II) removal from aqueous solution. *Ind. Eng. Chem. Res.* **2014**, *53*, 18481–18488. [CrossRef]
23. Ou, Q.; Zhou, L.; Zhao, S.; Geng, H.; Hao, J.; Xu, Y.; Chen, H.; Chen, X. Self-templated synthesis of bifunctional Fe_3O_4@$MgSiO_3$ magnetic sub-microspheres for toxic metal ions removal. *Chem. Eng. J.* **2012**, *180*, 121–127. [CrossRef]
24. Argane, R.; Benzaazoua, M.; Hakkou, R.; Bouamrane, A. Reuse of base-metal tailings as aggregates for rendering mortars: Assessment of immobilization performances and environmental behavior. *Constr. Build. Mater.* **2015**, *96*, 296–306. [CrossRef]
25. Zhao, Z.; Zhang, X.; Zhou, H.; Liu, G.; Kong, M.; Wang, G. Microwave-assisted synthesis of magnetic Fe_3O_4-mesoporous magnesium silicate core-shell composites for the removal of heavy metal ions. *Microporous Mesoporous Mater.* **2017**, *242*, 50–58. [CrossRef]
26. Gorakhki, M.H.; Bareither, C.A. Sustainable Reuse of Mine Tailings and Waste Rock as Water-Balance Covers. *Minerals* **2017**, *7*, 128. [CrossRef]
27. Aprianti, E. A huge number of artificial waste material can be supplementary cementitious material (SCM) for concrete production—A review part II. *J. Clean. Prod.* **2017**, *142*, 4178–4194. [CrossRef]
28. Qiu, H.; Lv, L.; Pan, B.; Zhang, Q.; Zhang, W.; Zhang, Q. Critical review in adsorption kinetic models. *J. Zhejiang Univ. A* **2009**, *10*, 716–724. [CrossRef]
29. Sverjensky, D.A.; Sahai, N. Theoretical prediction of single-site surface-protonation equilibrium constants for oxides and silicates in water. *Geochim. Cosmochim. Acta* **1996**, *60*, 3773–3797. [CrossRef]
30. Mohan, S.; Gandhimathi, R. Removal of heavy metal ions from municipal solid waste leachate using coal fly ash as an adsorbent. *J. Hazard. Mater.* **2009**, *169*, 351–359. [CrossRef]
31. Chaari, I.; Fakhfakh, E.; Chakroun, S.; Bouzid, J.; Boujelben, N.; Feki, M.; Rocha, F.; Jamoussi, F. Lead removal from aqueous solutions by a Tunisian smectitic clay. *J. Hazard. Mater.* **2008**, *156*, 545–551. [CrossRef]
32. Egodawatte, S.; Greenstein, K.E.; Vance, I.; Rivera, E.; Myung, N.V.; Parkin, G.F.; Cwiertny, D.M.; Larsen, S.C. Electrospun hematite nanofiber/mesoporous silica core/shell nanomaterials as an efficient adsorbent for heavy metals. *RSC Adv.* **2016**, *6*, 90516–90525. [CrossRef]
33. Zhang, Q.; Lin, B.; Hong, J.; Chang, C.T. Removal of ammonium and heavy metals by cost-effective zeolite synthesized from waste quartz sand and calcium fluoride sludge. *Water Sci. Technol.* **2017**, *75*, 587–597. [CrossRef] [PubMed]
34. Rethwisch, D.G.; Dumesic, J.A. Effect of Metal–Oxygen Bond Strength on Properties of Oxides. 1. Infrared Spectroscopy of Adsorbed CO and CO_2. *Langmuir* **1986**, *2*, 73–79. [CrossRef]
35. Al-Oweini, R.; El-Rassy, H. Synthesis and characterization by FTIR spectroscopy of silica aerogels prepared using several $Si(OR)_4$ and $R''Si(OR')_3$ precursors. *J. Mol. Struct.* **2009**, *919*, 140–145. [CrossRef]
36. Eren, E.; Afsin, B. An investigation of Cu(II) adsorption by raw and acid-activated bentonite: A combined potentiometric, thermodynamic, XRD, IR, DTA study. *J. Hazard. Mater.* **2008**, *151*, 682–691. [CrossRef]
37. Mcdowell, R.S.; Horrocks, W.D.; Yates, J.T. Infrared spectrum of $Co(CO)_3NO$. *J. Chem. Phys.* **1961**, *34*, 530–534. [CrossRef]
38. Bradl, H.B. Adsorption of heavy metal ions on soils and soils constituents. *J. Colloid Interface Sci.* **2004**, *277*, 1–18. [CrossRef] [PubMed]
39. Duan, P.; Yan, C.; Zhou, W.; Ren, D. Development of fly ash and iron ore tailing based porous geopolymer for removal of Cu(II) from wastewater. *Ceram. Int.* **2016**, *42*, 13507–13518. [CrossRef]
40. Jiang, M.Q.; Jin, X. ying; Lu, X.Q.; Chen, Z. liang Adsorption of Pb(II), Cd(II), Ni(II) and Cu(II) onto natural kaolinite clay. *Desalination* **2010**, *252*, 33–39. [CrossRef]
41. Wang, W.; Tian, G.; Zhang, Z.; Wang, A. A simple hydrothermal approach to modify palygorskite for high-efficient adsorption of Methylene blue and Cu(II) ions. *Chem. Eng. J.* **2015**, *265*, 228–238. [CrossRef]
42. Adebowale, K.O.; Unuabonah, I.E.; Olu-Owolabi, B.I. The effect of some operating variables on the adsorption of lead and cadmium ions on kaolinite clay. *J. Hazard. Mater.* **2006**, *134*, 130–139. [CrossRef]
43. Jin, X.; Yu, C.; Li, Y.; Qi, Y.; Yang, L.; Zhao, G.; Hu, H. Preparation of novel nano-adsorbent based on organic-inorganic hybrid and their adsorption for heavy metals and organic pollutants presented in water environment. *J. Hazard. Mater.* **2011**, *186*, 1672–1680. [CrossRef]
44. Vindevoghel, P.; Guyot, A. Suspended Emulsion Copolymerization of Acrylonitrile and Methyl Acrylate. *Polym. React. Eng.* **1995**, *3*, 23–42. [CrossRef]

45. Unuabonah, E.I.; Adebowale, K.O.; Olu-Owolabi, B.I.; Yang, L.Z.; Kong, L.X. Adsorption of Pb (II) and Cd (II) from aqueous solutions onto sodium tetraborate-modified Kaolinite clay: Equilibrium and thermodynamic studies. *Hydrometallurgy* **2008**, *93*, 1–9. [CrossRef]
46. Uddin, M.K. A review on the adsorption of heavy metals by clay minerals, with special focus on the past decade. *Chem. Eng. J.* **2017**, *308*, 438–462. [CrossRef]
47. Guo, S.; Dan, Z.; Duan, N.; Chen, G.; Gao, W.; Zhao, W. Zn (II), Pb (II), and Cd (II) adsorption from aqueous solution by magnetic silica gel: Preparation, characterization, and adsorption. *Environ. Sci. Pollut. Res.* **2018**, *25*, 30938–30948. [CrossRef]
48. Adebowale, K.O.; Unuabonah, I.E.; Olu-Owolabi, B.I. Adsorption of some heavy metal ions on sulfate- and phosphate-modified kaolin. *Appl. Clay Sci.* **2005**, *29*, 145–148. [CrossRef]
49. Zacaroni, L.M.; Magriotis, Z.M.; das Graças Cardoso, M.; Santiago, W.D.; Mendonça, J.G.; Vieira, S.S.; Nelson, D.L. Natural clay and commercial activated charcoal: Properties and application for the removal of copper from cachaça. *Food Control* **2015**, *47*, 536–544. [CrossRef]
50. Rao, M.; Parwate, A.V.; Bhole, A.G. Removal of Cr^{6+} and Ni^{2+} from aqueous solution using bagasse and fly ash. *Waste Manag.* **2002**, *22*, 821–830. [CrossRef]
51. Diamadopoulos, E. As (V) Removal from aqueous solutions by. *Water Res.* **1993**, *27*, 1773–1777. [CrossRef]
52. Gan, Q. A case study of microwave processing of metal hydroxide sediment sludge from printed circuit board manufacturing wash water. *Waste Manag.* **2000**, *20*, 695–701. [CrossRef]
53. Lopez, E.A.; Perez, C. The adsorption of copper (11) ions from aqueous solution on blast furnace sludge. *J. Mater. Sci. Lett.* **1996**, *15*, 1310–1312. [CrossRef]
54. Zhai, Y.; Wei, X.; Zeng, G.; Zhang, D.; Chu, K. Study of adsorbent derived from sewage sludge for the removal of Cd^{2+}, Ni^{2+} in aqueous solutions. *Sep. Purif. Technol.* **2004**, *38*, 191–196. [CrossRef]
55. Srivastava, S.; Gupta, V.K.; Mohan, D. Removal of lead and chromium by activated slag-A blast-Furnace waste. *J. Environ. Eng.* **1997**, *123*, 461–468. [CrossRef]
56. Papandreou, A.; Stournaras, C.J.; Panias, D. Copper and cadmium adsorption on pellets made from fired coal fly ash. *J. Hazard. Mater.* **2007**, *148*, 538–547. [CrossRef]
57. Treybal, R.E. *Tryball, Mass Transfers Operations*, 3rd ed.; McGraw: New York, NY, USA, 1980.
58. Juang, R.S.; Wu, F.C.; Tseng, R.L. The Ability of Activated Clay for the Adsorption of Dyes from Aqueous Solutions. *Environ. Technol.* **1997**, *18*, 525–531. [CrossRef]
59. Shahbazi, A.; Younesi, H.; Badiei, A. Functionalized SBA-15 mesoporous silica by melamine-based dendrimer amines for adsorptive characteristics of Pb(II), Cu(II) and Cd(II) heavy metal ions in batch and fixed bed column. *Chem. Eng. J.* **2011**, *168*, 505–518. [CrossRef]
60. Nguyen, T.C.; Loganathan, P.; Nguyen, T.V.; Vigneswaran, S.; Kandasamy, J.; Naidu, R. Simultaneous adsorption of Cd, Cr, Cu, Pb, and Zn by an iron-coated Australian zeolite in batch and fixed-bed column studies. *Chem. Eng. J.* **2015**, *270*, 393–404. [CrossRef]